PCP
PLANT & CELL PHYSIOLOGY

Regular Paper

# Exploiting the Substrate Promiscuity of Hydroxycinnamoyl-CoA:Shikimate Hydroxycinnamoyl Transferase to Reduce Lignin

Aymerick Eudes[1,2], Jose H. Pereira[1,3], Sasha Yogiswara[1,2,4], George Wang[1,2], Veronica Teixeira Benites[1,2,5], Edward E.K. Baidoo[1,2], Taek Soon Lee[1,2], Paul D. Adams[1,3], Jay D. Keasling[1,2,4] and Dominique Loqué[1,2,*]

[1]Joint BioEnergy Institute, EmeryStation East, 5885 Hollis St, 4th Floor, Emeryville, CA 94608, USA
[2]Biological Systems and Engineering Division, Lawrence Berkeley National Laboratory, 1 Cyclotron Road, Berkeley, CA 94720, USA
[3]Molecular Biophysics and Integrated Bioimaging Division, Lawrence Berkeley National Laboratory, 1 Cyclotron Road, Berkeley, CA 94720, USA
[4]Department of Bioengineering & Department of Chemical & Biomolecular Engineering, University of California, Berkeley, CA 94720, USA
[5]Graduate Program, San Francisco State University, San Francisco, CA 94132, USA
*Corresponding author: E-mail, dloque@lbl.gov; Fax, +1-510-486-4252.
(Received August 6, 2015; Accepted January 13, 2016)

**Lignin poses a major challenge in the processing of plant biomass for agro-industrial applications. For bioengineering purposes, there is a pressing interest in identifying and characterizing the enzymes responsible for the biosynthesis of lignin. Hydroxycinnamoyl-CoA:shikimate hydroxycinnamoyl transferase (HCT; EC 2.3.1.133) is a key metabolic entry point for the synthesis of the most important lignin monomers: coniferyl and sinapyl alcohols. In this study, we investigated the substrate promiscuity of HCT from a bryophyte (*Physcomitrella*) and from five representatives of vascular plants (Arabidopsis, poplar, switchgrass, pine and *Selaginella*) using a yeast expression system. We demonstrate for these HCTs a conserved capacity to acylate with *p*-coumaroyl-CoA several phenolic compounds in addition to the canonical acceptor shikimate normally used during lignin biosynthesis. Using either recombinant HCT from switchgrass (PvHCT2a) or an Arabidopsis stem protein extract, we show evidence of the inhibitory effect of these phenolics on the synthesis of *p*-coumaroyl shikimate in vitro, which presumably occurs via a mechanism of competitive inhibition. A structural study of PvHCT2a confirmed the binding of a non-canonical acceptor in a similar manner to shikimate in the active site of the enzyme. Finally, we exploited in Arabidopsis the substrate flexibility of HCT to reduce lignin content and improve biomass saccharification by engineering transgenic lines that overproduce one of the HCT non-canonical acceptors. Our results demonstrate conservation of HCT substrate promiscuity and provide support for a new strategy for lignin reduction in the effort to improve the quality of plant biomass for forage and cellulosic biofuels.**

**Keywords:** Arabidopsis • Bioenergy • Cell wall • HCT • Lignin • Saccharification.

**Abbreviations:** 4CL5, Arabidopsis 4-coumarate-CoA ligase 5; C3′H, *p*-coumaroyl shikimate 3′-hydroxylase; CSE, caffeoyl shikimate esterase; ESI-TOF, electrospray ionization-time-of-flight; HCT, hydroxycinnamoyl-CoA:shikimate hydroxycinnamoyl transferase; LC-MS/MS, liquid chromatography–tandem mass spectrometry; RT–PCR, reverse transcription–PCR; YNB: yeast nitrogen base.

## Introduction

Plant biomass is routinely utilized in diverse agro-industrial sectors such as pulp and paper, forage, bio-manufacturing and bioenergy. Among several sustainable energy strategies, the conversion of plant cell walls into fermentable sugars offers the possibility for microbial production of bio-based products including materials (e.g. biopolymers), commodity chemicals, fine and specialty chemicals, and liquid fuels (Vickers et al. 2012, George et al. 2015). Lignin is a hydrophobic polymer that permeates plant cell walls and impedes the biochemical processes used for plant biomass conversion into fermentable sugars (Zeng et al. 2014). Lignin from ferns and gymnosperms contains *p*-hydroxyphenyl (H) and guaiacyl (G) units derived from *p*-coumaroyl alcohol and coniferyl alcohol, respectively; and lignin from certain lycophytes and angiosperms additionally contains syringyl (S) units (Boerjan et al. 2003, Weng et al. 2010). These lignin monomers (or monolignols) are synthesized from phenylalanine in the cytosol and exported to the cell wall for oxidative polymerization (Boerjan et al. 2003).

In the lignin pathway, the metabolic entry point responsible for the production of both coniferyl and sinapyl alcohols involves hydroxycinnamoyl-CoA:shikimate hydroxycinnamoyl transferase (HCT), which catalyzes the coupling of *p*-coumaroyl-CoA with shikimate to produce *p*-coumaroyl shikimate (**Fig. 1**) (Hoffman et al. 2003, Hoffman et al. 2004). Following this step, the hydroxycinnamoyl moiety of *p*-coumaroyl shikimate is hydroxylated by *p*-coumaroyl shikimate 3′-hydroxylase (C3′H) to produce caffeoyl shikimate which is then transesterified by HCT to release caffeoyl-CoA, or, as recently described in Arabidopsis, cleaved by caffeoyl shikimate esterase (CSE) to release caffeate (**Fig. 1**) (Franke et al. 2002, Vanholme et al. 2013a). Reduction of HCT activity limits the synthesis of coniferyl and sinapyl alcohols and causes a backlog of upstream metabolites,

*Plant Cell Physiol.* 57(3): 568–579 (2016) doi:10.1093/pcp/pcw016, Advance Access publication on 8 February 2016, available online at www.pcp.oxfordjournals.org

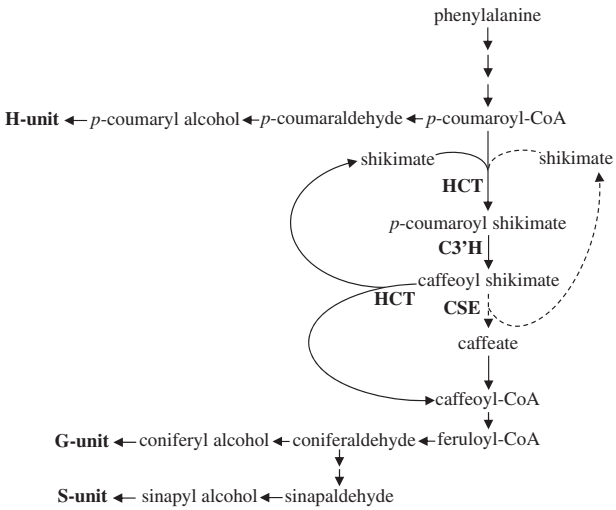


**Fig. 1** Simplified representation of the lignin biosynthetic pathway. Abbreviations: HCT, hydroxycinnamoyl-CoA:shikimate hydroxycinnamoyl transferase; C3′H, *p*-coumaroyl shikimate 3′-hydroxylase; CSE, caffeoyl shikimate esterase. Dashed arrows represent the CSE-mediated esterification of caffeoyl shikimate as described in Arabidopsis (Vanholme et al. 2013a).

which leads to a redirection of part of the metabolic flux of *p*-coumaroyl-CoA into *p*-coumaryl alcohol. Therefore, the lignin from plants exhibiting strong HCT down-regulation is enriched in H units and its content is heavily reduced due to the poor capacity of *p*-coumaroyl alcohol to incorporate the polymer (Hoffman et al. 2004, Vanholme et al. 2013b). Considering its central role in lignin biosynthesis, HCT has been a target in genetic engineering strategies for improving the commercial utility of plant biomass. For example, down-regulation of *HCT* expression reduces lignin content and improves forage digestibility and saccharification efficiency in alfalfa (Chen and Dixon 2007, Shadle et al. 2007).

HCT belongs to the BAHD family of acyl-CoA-dependent transferases, which includes several enzymes that use hydroxycinnamoyl-CoAs as a donor for the transfer reaction (D'Auria 2006). These transferases are capable of acylating a wide variety of acceptors, and some of them exhibit broad substrate flexibility (Landmann et al. 2011, Molina and Kosma 2014). For example, it is well known that some HCTs can use quinate as a substrate in addition to shikimate (Hoffman et al. 2003, Lallemand et al. 2012, Walker et al. 2013, Escamilla-Treviño et al. 2014). Moreover, HCT from globe artichoke (CcHCT) was shown to accept 3-hydroxyanthranilate as a substrate (Moglia et al. 2010), and similar substrate promiscuity was described for HCT from *Coleus blumei*, which can also use 3-amino- and 3-hydroxybenzoates as acceptor substrates, forming both *p*-coumarate ester and amide conjugates (Sander and Petersen 2011). Although HCT is a well-conserved enzyme among land plants (Xu et al. 2009, Tohge et al. 2013), characterization of its substrate flexibility remains poorly described. Furthermore, until now, it had yet to be tested whether the substrate promiscuity of HCT could be exploited for lignin engineering and improving plant biomass.

In this study, using a yeast expression system, we investigated the substrate promiscuity of HCT from a bryophyte (*Physcomitrella patens*), a lycophyte (*Selaginella moellendorffii*), a coniferous gymnosperm (*Pinus radiata*), a monocot angiosperm (*Panicum virgatum*) and two dicot angiosperms (*Populus trichocarpa* and *Arabidopsis thaliana*) toward a series of benzene and benzoate derivatives. Recombinant yeast strains that individually co-express these phylogenetically related HCTs with 4-coumarate-CoA ligase were capable of producing *p*-coumaroyl conjugates when fed with *p*-coumarate and shikimate, 3-hydroxybenzoate, 2,5-dihydroxybenzoate (gentisate), 2,3-dihydroxybenzoate, 3,4-dihydroxybenzoate (protocatechuate), 3-aminobenzoate, 3-hydroxyanthranilate, 5-hydroxyanthranilate, *ortho*-hydroxyphenol (catechol) and *para*-hydroxyphenol (hydroquinone). Purified recombinant HCT from switchgrass showed activity towards these new 'non-canonical' substrates, which confirmed their capacity to bind the active site of the enzyme. Moreover, we demonstrate that in vitro formation of *p*-coumaroyl shikimate by either a switchgrass recombinant HCT (PvHCT2a) or an Arabidopsis stem protein extract is partially inhibited in the presence of the non-canonical acceptors, presumably via a mechanism of competitive inhibition. Finally, we extended this characterization to in vivo inhibition assays by engineering Arabidopsis lines to overproduce one of these HCT-competitive inhibitors (protocatechuate) in lignifying tissues, and showed an approximately 30% reduction of lignin content, providing a significant improvement of biomass saccharification efficiency. Our results demonstrate the potential of inhibiting HCT in various bioenergy crops by overproducing unusual HCT acceptors in planta. The substrate promiscuity of HCT was observed in all the plant taxa we tested, and it appears to have been conserved since plants first appeared on land about 450 Ma ago. This novel approach could be particularly valuable to reduce lignin in crops for which genomic information is still unavailable.

## Results

### Selection and identification of HCT sequences

For this study, we selected HCT from Arabidopsis (AtHCT) since it has been shown to be genetically implicated in lignin biosynthesis (Hoffman et al. 2004). A HCT from the woody dicot poplar was also selected. In particular, out of seven HCT genes found in the poplar genome, *PtHCT1* and *PtHCT6* have been associated with lignin biosynthesis because of their xylem-specific expression profile (Shi et al. 2010). PtHCT6 was selected for this study since it has higher catalytic efficiency towards coumaroyl-CoA (Wang et al. 2014). In the monocot switchgrass, two enzymes (PvHCT1a and PvHCT2a) have proven HCT activity (Escamilla-Treviño et al. 2014). PvHCT2a was selected for this study based on its predicted involvement in lignin biosynthesis according to gene expression profiling experiments (Shen et al. 2013). For gymnosperms, we selected a HCT from pine (PrHCT) for which the silencing in cell cultures results in reduction of lignin content (Wagner et al. 2007). Moreover, we conducted a phylogenetic analysis using

biochemically characterized hydroxycinnamoyl-CoA-dependent BAHD transferases (**Supplementary Table S1**) and confirmed that AtHCT, PtHCT6, PvHCT2a and PrHCT belong to the same clade along with other characterized HCTs (**Supplementary Fig. S1**). In order to include a HCT from a lycophyte, we searched the *S. moellendorffii* genome for the presence of putative HCT homologs using AtHCT as bait. Five sequences were retrieved by selecting proteins whose sequence share at least 35% identity with that of AtHCT, and two of which, SmHCT1a and SmHCT1b (60% and 61% identical to AtHCT, respectively), fall into the 'HCT clade' (**Supplementary Table S1**; **Supplementary Fig. S1**). These two proteins (98% identical) are products of allelic variants of the same gene, and SmHCT1a was selected for further characterization. Similarly, the genome of the bryophyte *P. patens* was analyzed for the identification of putative HCT homologs using AtHCT as bait. Out of the seven sequences retrieved (using a protein sequence identity cut-off of 30%), one protein (PpHCT1) falls into the 'HCT clade' and was selected for this study (**Supplementary Table S1**; **Supplementary Fig. S1**).

## Screening of HCT substrate promiscuity using a yeast heterologous expression system

AtHCT, PtHCT6, PvHCT2a and PrHCT, as well as putative HCTs from *S. moellendorffii* (SmHCT1a) and *P. patens* (PpHCT1), were individually co-expressed with Arabidopsis 4-coumarate-CoA ligase 5 (4CL5) in yeast to investigate their substrate affinity toward various acceptors. In these in vivo assays, the different recombinant yeast strains were fed individually with *p*-coumarate in combination with shikimate (as a positive control) or one of the potential phenolic acceptors listed in **Supplementary Fig. S2**. These acceptors were chosen based on previous reports that assign this type of alternative substrates for HCT (Moglia et al. 2010, Sander and Petersen, 2011). 4CL5 converts *p*-coumarate into *p*-coumaroyl-CoA, which is in turn coupled to shikimate or other potential acceptors by HCT. Subsequently, we performed liquid chromatography–tandem mass spectrometry (LC-MS/MS) analysis of the yeast culture medium for the detection of *p*-coumaroyl conjugates produced by the different HCTs. Out of 20 phenolics tested, the analysis indicated that all six HCTs produced *p*-coumaroyl conjugates in the presence of shikimate, 3-hydroxybenzoate, gentisate, 2,3-dihydroxybenzoate, protocatechuate, 3-aminobenzoate, 3-hydroxyanthranilate, 5-hydroxyanthranilate, catechol and hydroquinone (**Fig. 2**; **Supplementary Table S2**; **Supplementary Fig. S3**). None of these products was found in the culture medium of a control yeast strain expressing 4CL5 alone and fed with *p*-coumarate and the corresponding acceptors. For these yeast-feeding assays, the limited control of enzyme expression, substrate penetrability and secretion of products does not allow direct comparisons of activities between the different HCTs and the various acceptors tested.

## Activity and inhibition of recombinant HCT

PvHCT2a was expressed in *Escherichia coli* and purified to confirm its activity towards shikimate and the nine new acceptors identified with the yeast screen. PvHCT2a was selected for biochemical assays since its expression in *E. coli* yielded pure and high amounts of recombinant enzyme (**Supplementary Fig. S4**), as opposed to the yield obtained using AtHCT which was expressed almost entirely as insoluble inclusion bodies. Conclusively, incubations of recombinant PvHCT2a with *p*-coumaroyl-CoA and shikimate, gentisate, 3-hydroxyanthranilate, 2,3-dihydroxybenzoate, catechol, protocatechuate, 5-hydroxyanthranilate, 3-hydroxybenzoate, 3-aminobenzoate and hydroquinone resulted in the formation of the corresponding *p*-coumaroyl conjugates (**Supplementary Fig. S5**). The chromatographic peaks of these PvHCT2a products showed retention times similar to those of the *p*-coumaroyl conjugates previously characterized in the yeast feedings. In contrast, incubations of PvHCT2a with only *p*-coumaroyl-CoA, or just the different acceptors, did not produce any of these reaction products (data not shown). Assuming similar LC-MS/MS response factors for the different *p*-coumaroyl conjugates, comparison of their peak intensities obtained from PvHCT2a in vitro assays showed that shikimate is the best substrate, followed by 3-hydroxyanthranilate (**Supplementary Fig. S6**). Substrate saturation curves using shikimate or the non-canonical acceptors were attempted to determine the affinity of PvHCT2a for these different substrates. Apparent substrate saturation of the enzyme could be achieved only in the case of shikimate, 3-hydroxyanthranilate and protocatechuate; double reciprocal plots indicated $K_m$ values of 699 μM, 830 μM and 1.48 mM, respectively, for these three acceptors (**Supplementary Fig. S7**). For the other acceptors, the lack of enzyme saturation at high concentrations indicates higher $K_m$ values and much lower affinity of PvHCT2a for these substrates compared with shikimate (**Supplementary Fig. S7**).

Because HCT acylates non-canonical acceptors in the presence of *p*-coumaroyl-CoA, we tested the influence of these potential competitive inhibitors on the formation of *p*-coumaroyl shikimate catalyzed by PvHCT2a in vitro. We observed that *p*-coumaroyl shikimate synthesis was reduced in reactions containing *p*-coumaroyl-CoA and an equimolar amount of shikimate and the non-canonical acceptors, in comparison with control reactions containing only *p*-coumaroyl-CoA and shikimate. In particular, inhibitions of *p*-coumaroyl shikimate synthesis ranged from 11% to 48%, depending on the acceptors present, and were stronger at higher concentrations (**Fig. 3**). In these reactions, the presence of *p*-coumaroyl conjugates formed from the coupling of *p*-coumaroyl-CoA with the non-canonical acceptors was also detected in addition to *p*-coumaroyl shikimate (data not shown).

## PvHCT2a substrate-binding site

The structure of the related HCT from *Sorghum bicolor* (SbHCT) has been described previously (Walker et al. 2013). As expected, the PvHCT2a structure consists of two domains, with the *p*-coumaryl-CoA- and shikimate-binding sites located between them. Domain I consists of N-terminal residues 1–199 and C-terminal residues 387–409. Domain II consists exclusively of C-terminal residues 200–386 and 410–446 (**Fig. 4A**). The structure of PvHCT2a in complex with *p*-coumaroyl-CoA and

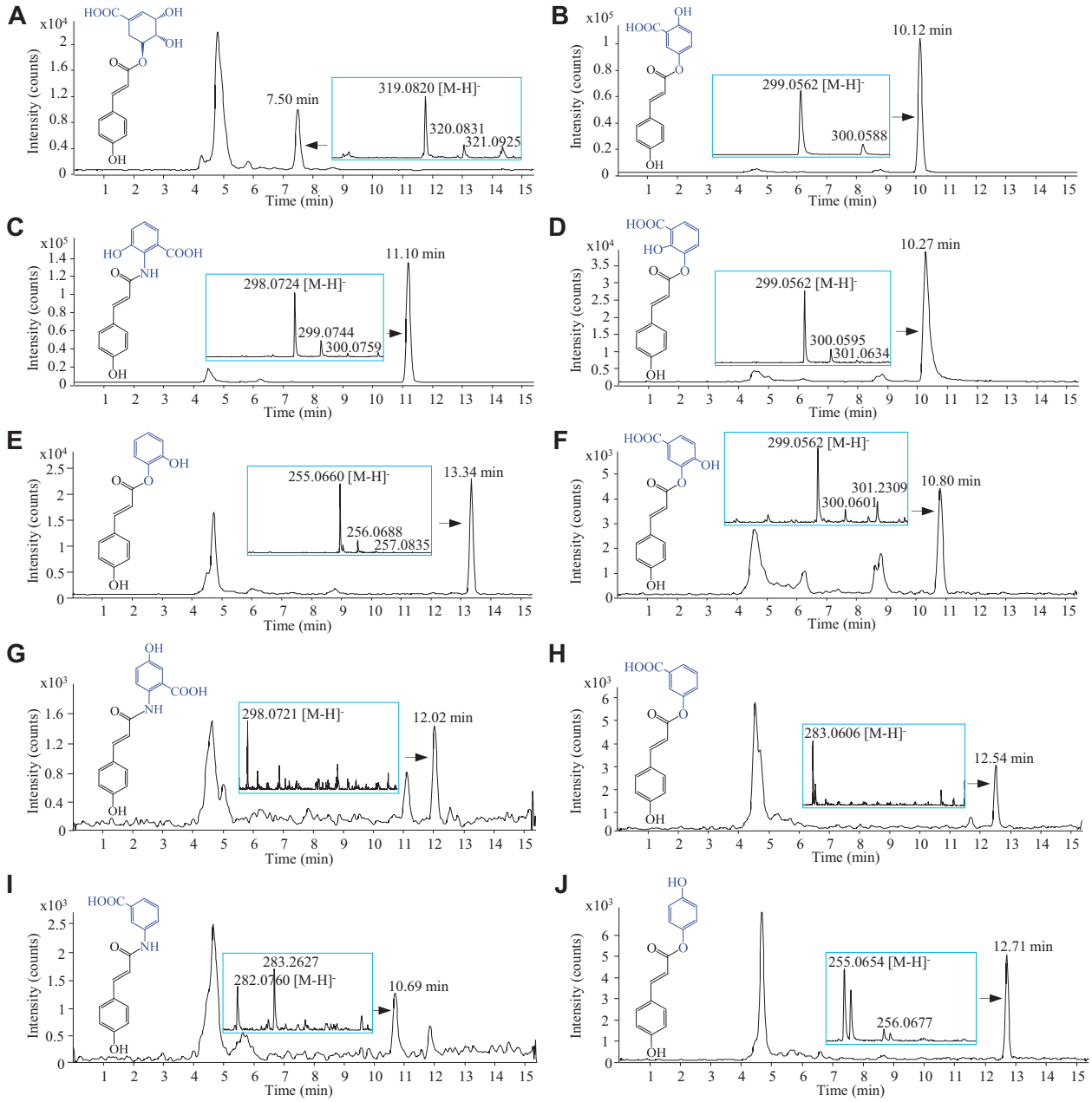


**Fig. 2** *p*-Coumaroyl conjugates produced by PvHCT2a in vivo activity assays. Representative LC-MS chromatograms of *p*-coumaroyl conjugates produced by PvHCT2a after feeding the recombinant yeast strains co-expressing At4CL5 and PvHCT2a with *p*-coumarate and (A) shikimate, (B) gentisate, (C) 3-hydroxyanthranilate, (D) 2,3-dihydroxybenzoate, (E) catechol, (F) protocatechuate, (G) 5-hydroxyanthranilate, (H) 3-hydroxybenzoate, (I) 3-aminobenzoate and (J) hydroquinone. Structures of *p*-coumaroyl hydroxybenzoates (B, D, F) are arbitrarily shown with an ester linkage involving the hydroxyl group on the C3 position on the carbon ring. The structure of *p*-coumaroyl 3-hydroxyanthranilate (C) is represented as determined in Moglia et al. (2010). See also **Table S2**.

shikimate reveals that the two molecules reacted during the soaking of the compounds into the crystal. Therefore, the product state was observed in the electron density map, given the ternary complex of PvHCT2a, free CoA and *p*-coumaroyl shikimate (**Fig. 4B**). A similar product state formation of *p*-coumaroyl shikimate was described for the related structure SbHCT (Walker et al. 2013). In contrast, our crystal structure of PvHCT2a–*p*-coumaroyl-CoA–protocatechuate is in a substrate state, i.e. the ternary complex consists of PvHCT2a, *p*-coumaroyl-CoA and protocatechuate (**Fig. 4C**). Data collection, refinement and model statistics for both PvHCT2a–*p*-coumaroyl-CoA–shikimate and PvHCT2a–*p*-coumaroyl-CoA–protocatechuate structures are summarized in **Supplementary Table S3**.

The *p*-coumaroyl-shikimate contacts the PvHCT2a via the phenolic group and carbonyl group of the *p*-coumaroyl portion. The shikimate portion contacts PvHCT2a through both the carboxyl and hydroxyl groups. The carbonyl group of the *p*-coumaroyl moiety directly contacts Trp384 and the phenolic moiety interacts via water-mediated hydrogen bonds with

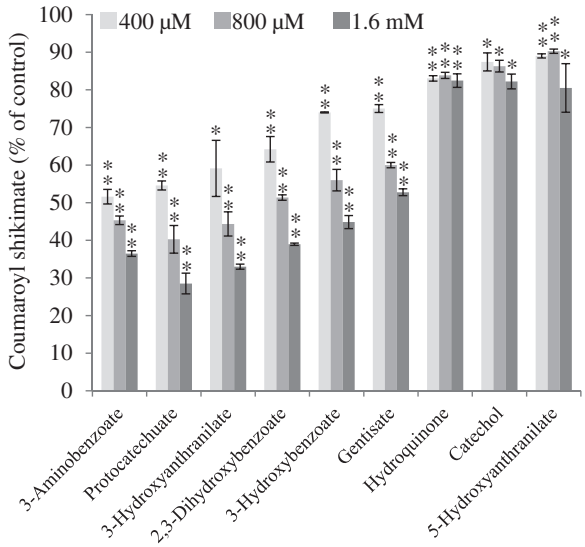


**Fig. 3** Inhibition of HCT activity in vitro. Production of *p*-coumaroyl shikimate by recombinant PvHCT2a using *p*-coumaroyl-CoA and shikimate as substrates (400 µM each) was measured in the absence (control) or presence of various concentrations of 3-aminobenzoate, protocatechuate, 3-hydroxyanthranilate, 2,3-dihydroxybenzoate, 3-hydroxybenzoate, gentisate, hydroquinone, catechol or 5-hydroxyanthranilate. Asterisks indicate significant differences from the control using the unpaired Student's *t*-test (**$P < 0.005$, *$P < 0.05$).

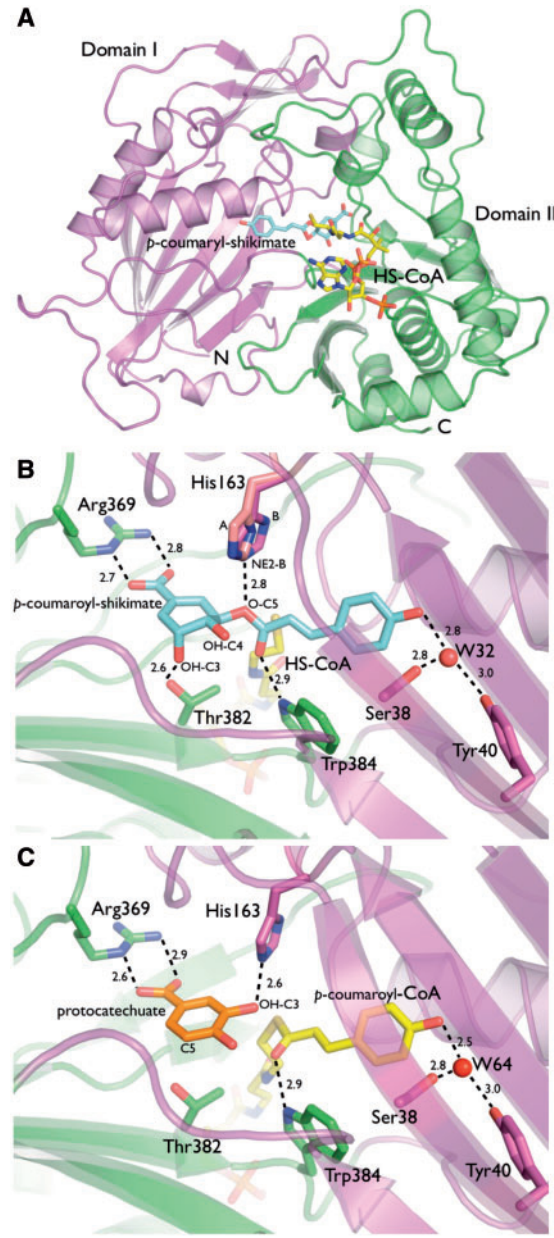


**Fig. 4** Structural study of PvHCT2a. (A) Cartoon representation of the monomeric PvHCT2a structure. The overall structure of PvHCT2a consists of two domains with the *p*-coumaroyl-CoA- and shikimate-binding site located between the domains. Each of the domains contains a core β-sheet surrounded by α-helices. (B) Substrate-binding site of the PvHCT2a–*p*-coumaroyl-CoA–shikimate ternary complex. The residues Arg369, Thr382, His163 and Trp384 interact directly with *p*-coumaroyl shikimate. The residues Ser38 and Tyr40 interact via water- (W32) mediated hydrogen bonds with *p*-coumaroyl shikimate. The His163 residue was observed in two alternative conformations represented in magenta and pink. (C) Substrate-binding site of the PvHCT2a–*p*-coumaroyl-CoA–protocatechuate ternary complex. The major difference between protocatechuate and shikimate binding is the loss of the C5 hydroxyl interaction with Thr382.

Ser38 and Tyr40. The carboxyl group of the shikimate moiety makes a salt bridge interaction with Arg369. While the C5 hydroxyl group contacts the catalytic residue His163, the C3 hydroxyl group contacts Thr382 (**Fig. 4B**).

We then analyzed the structure of the protocatechuate ternary complex to better understand the mechanism of PvHCT2a. The protocatechuate binds in a very similar manner to shikimate, with the carboxyl group making a tight salt bridge with Arg369, and the C3 (equivalent to C5 in the shikimate moiety) hydroxyl group interacting with the nitrogen NE2 of His163. However, we see that the C5 (equivalent to C3 in the shikimate moiety) hydroxyl interaction with Thr382 is lost, since this hydroxyl group is absent in protocatechuate (**Fig. 4C**).

## Characterization of Arabidopsis lines producing a competitive inhibitor of HCT in lignifying tissues

As a preliminary experiment, we determined the influence of the alternative HCT acceptors on the formation of *p*-coumaroyl shikimate catalyzed by a total protein extract from Arabidopsis stems. Compared with control reactions containing only *p*-coumaroyl-CoA and shikimate, and except for catechol and 5-hydroxyanthranilate, we observed reductions of *p*-coumaroyl shikimate synthesis ranging from 6.0% to 63.5% in reactions containing equimolar amount of the different non-canonical substrates, and the strongest inhibition was observed with protocatechuate (**Supplementary Fig. S8**).

Since the synthesis of *p*-coumaroyl shikimate by protein extracts from Arabidopsis stems is strongly inhibited by protocatechuate in vitro, we attempted to generate Arabidopsis transgenic lines that overproduce protocatechuate from chorismate to reduce lignin content. A two-gene strategy was employed to convert some of the endogenous chorismate pool into *p*-hydroxybenzoate—and eventually protocatechuate by co-expressing chorismate pyruvate-lyase from *E. coli* (ubiC)

and *p*-hydroxybenzoate 3-monooxygenase from *Pseudomonas aeruginosa* (pobA) (**Fig. 5A**). In Arabidopsis lignifying tissues, the promoter of the secondary cell wall cellulose synthase gene *AtCesa4* was used to drive the expression of *ubiC*, while the promoter of the cinnamate 4-hydroxylase gene *AtC4H*, involved in the lignin biosynthetic pathway, was used to drive the expression of *pobA*. Two different promoters were used to minimize gene silencing effects that could potentially arise from the expression of identical 5′-untranslated region (UTR) sequences. Moreover, using an N-terminal fusion with a sequence encoding a plastid-targeting signal peptide, both ubiC and pobA were targeted to the plastids in which chorismate is produced. Two lines harboring a T-DNA carrying either *ubiC* alone (*ubiC-1* and *ubiC-2*) or *pobA* alone (*pobA-1* and *pobA-2*), and three lines harboring a T-DNA carrying both genes (*ubiC-pobA-1*, *-2* and *-3*) were selected for characterization. Reverse transcription–PCR (RT–PCR) showed the expression of only *ubiC* or *pobA* in the *ubiC-1*, *-2* lines and *pobA-1*, *-2* lines, respectively, and expression of both genes in the three *ubiC-pobA* lines (**Fig. 5B**). Methanol-soluble metabolites were extracted from stems of the transgenic lines, and both *p*-hydroxybenzoate and protocatechuate were quantified using LC-MS/MS. The metabolite analysis showed a higher amount of *p*-hydroxybenzoate in the *ubiC-1* and *-2* lines compared with the wild type (7.5- and 6.8-fold higher, respectively), while the levels observed in the *ubiC-pobA* lines were similar to those of the wild type. In contrast, the protocatechuate content was 24- to 26-fold higher in the *ubiC-pobA* lines compared with the wild-type and the *ubiC* lines (**Fig. 5C**). These results confirmed the production of *p*-hydroxybenzoate from chorismate by ubiC activity and its efficient conversion to protocatechuate by pobA in the *ubiC-pobA* transgenic lines. In addition, measurement of phenylalanine—an amino acid derived from chorismate and precursor of monolignols—and salicylic acid contents revealed no significant difference between the wild type and transgenic lines (**Supplementary Table S4**).

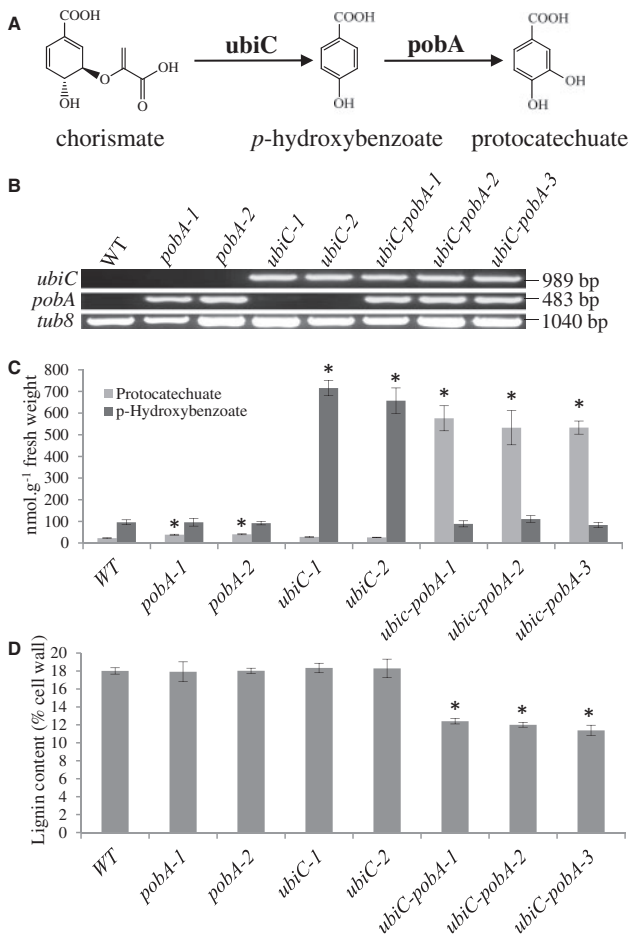


**Fig. 5** Characterization of transgenic Arabidopsis lines accumulating protocatechuate. (A) Strategy used for the conversion of chorismate into protocatechuate via *p*-hydroxybenzoate. (B) Detection by RT–PCR of *ubiC* and *pobA* transcripts using stem mRNA from 5-week-old wild-type (WT), *pobA*, *ubiC* and *ubiC-pobA* transgenic lines. *Tub8*-specific primers were used to assess cDNA quality for each sample. (C) *p*-Hydroxybenzoate and protocatechuate contents in stems from 5-week-old WT, *pobA*, *ubiC* and *ubiC-pobA* transgenic lines. Bars represent the SE from four biological replicates ($n = 4$). Asterisks indicate significant differences from the wild type using the unpaired Student's *t*-test (*$P < 0.005$). (D) Lignin content in senesced mature stems from WT, *pobA*, *ubiC* and *ubiC-pobA* transgenic lines. Values in parentheses are the SE from biological replicates ($n = 13$ for the WT, $n = 4$ for *ubiC-pobA-1* and *-2*, $n = 3$ for *ubiC-1* and *-2*, *pobA-1* and *-2*, and *ubiC-pobA-3*). Asterisks indicate significant differences from the WT using the unpaired Student's *t*-test (*$P < 0.001$).

## Protocatechuate overproducer lines show reduction of lignin and improved biomass saccharification

Lignin content was measured from the stem biomass of senesced mature wild-type, *ubiC*, *pobA* and *ubiC-pobA* plants using the Klason method. In comparison with the wild type, lignin reductions of 31–37% were measured in the *ubiC-pobA* lines, whereas no decrease of lignin content was observed in the *ubiC* and *pobA* single lines (**Fig. 5D**). In addition, a reduction in stem height at maturity was noticeable for all three *ubiC-pobA* lines at late development stages compared with the single transgenic lines and wild-type plants (**Supplementary Fig. S9**). Lastly, using pyrolysis–gas chromatography (GC)/MS, we determined that the monomeric composition of lignin was altered in the *pobA-ubiC* lines, showing an increased S:G ratio as a result of higher and lower relative amount of S and G units, respectively (**Table 1**; **Supplementary Table S5**).

**Table 1** Lignin composition in senesced mature stems from wild-type (WT) and *ubiC-pobA* plants

| | %H | %G | %S | S/G |
|---|---|---|---|---|
| WT | 4.4 (0.2) | 60.4 (0.8) | 35.2 (0.6) | 0.58 |
| *ubiC-pobA-1* | 5.1 (0.0) | 41.6 (0.3)* | 53.3 (0.3)* | 1.28* |
| *ubiC-pobA-2* | 5.0 (0.4) | 42.6 (0.2)* | 52.3 (0.5)* | 1.23* |
| *ubiC-pobA-3* | 4.8 (0.4) | 46.7 (0.1)* | 48.4 (0.3)* | 1.04* |

Values in parenthests are the SE from biological replicates ($n = 7$ for the WT, $n = 4$ for *ubiC-pobA-1* and *-2*, $n = 3$ for *ubiC-pobA-3*).
Asterisks indicate significant differences from the WT using the unpaired Student's *t*-test (*$P < 0.001$).
See also **Supplementary Table S2**.

Saccharification assays on stem material were conducted to evaluate the potential of our approach to reduce overall biomass recalcitrance and engineer forage and bioenergy crops. As shown in **Fig. 6**, higher amounts of sugars were released from the biomass of the three *ubiC-pobA* lines, which exhibited saccharification improvements of 24–26% compared with the wild type during a 96 h enzymatic hydrolysis.

## Discussion

The substrate promiscuity of HCT was demonstrated by its capacity to form *p*-coumaroyl conjugates using various acceptors other than shikimate. This substrate flexibility appears conserved between HCTs from different representatives of land plants, occurring at least in one bryophyte and one lycophyte, as well as in euphyllophytes including one gymnosperm, one monocot angiosperm and two dicot angiosperms. Although *P. patens* contains orthologs of all the genes required for the synthesis of *p*-coumaryl and coniferyl alcohols (Xu et al. 2009), the presence of lignified tissues has never been demonstrated in this plant. We show here that *P. patens* possesses a bona fide HCT, but its physiological role remains unclear. Although PpHCT1 falls into the clade of known HCTs in the phylogenetic tree of hydroxycinnamoyl-CoA-dependent BAHD transferases (**Supplementary Fig. S1**), it may instead be involved in the synthesis of alternative phenylpropanoid conjugates such as chlorogenic acid (3-*O*-caffeoylquinic acid) which has been identified in *P. patens* (Erxleben et al. 2012). Moreover, this is, to our knowledge, the first demonstration of HCT activity for an enzyme from *Selaginella*. However, its involvement in lignification remains questionable due to the presence in this plant of a dual *meta*-hydroxylase (SmF5H), which can by-pass the enzymatic steps catalyzed by C3′H and HCT (Weng et al. 2010). More generally, BAHD acyltransferases from *Selaginella* could have a role in the synthesis of phenolic esters other than *p*-coumaroyl shikimate (Weng and Noel 2013).

Although the formation of *p*-coumaroyl shikimate occurs via an ester linkage between *p*-coumaroyl-CoA and shikimate, these HCTs can also catalyze the formation of *p*-coumaroyl conjugates via an amide bond, as exemplified with the use of 3-aminobenzoate as acceptor. Both ester and amide linkages are possible for the formation of *p*-coumaroyl 3-hydroxyanthranilate and *p*-coumaroyl 5-hydroxyanthranilate, but only one product was observed in our assays when these acceptors were tested. For these two cases, an amide bond can be anticipated, as previously determined for the *p*-coumarate conjugate formed by CcHCT using 3-hydroxyanthranilate (Moglia et al. 2010). In this work, the apparent $K_m$ value observed for PvHCT2a towards shikimate (~700 μM) is comparable with the values observed for tobacco HCT (750 μM), which has been genetically implicated in lignin biosynthesis (Hoffmann et al. 2003), and for poplar HCT (895 μM; Kim et al. 2011), but higher than the values reported for HCT from coffee (75 μM; Lallemand et al. 2012), sorghum (153 μM; Walker et al. 2013) and *Coleus blumei* (332 μM; Sander and Petersen 2011). The slightly different structure of the new HCT acceptors described in this study could influence their binding to the active site of the enzyme and explain the higher apparent $K_m$ values of HCT for these substrates compared with shikimate.

The catalytic mechanism of HCT has been elegantly described previously by Walker et al. (2013). In their mutagenesis experiments using shikimate as a substrate, the mutant T384A-SbHCT (equivalent to Thr382 in PvHCT2a) showed only 9% of the enzyme activity compared with wild-type SbHCT (Walker et al. 2013). We therefore propose that the loss of the C5 hydroxyl interaction with Thr382 in the PvHCT2a–*p*-coumaroyl-CoA–protocatechuate complex affected the effective binding of protocatechuate, thus engendering a similar effect to the T384A mutation in SbHCT on the turnover rate of the substrate. This is most probably the reason why it was possible to capture crystallographically the substrate PvHCT2a–*p*-coumaryl-CoA–protocatechuate ternary complex, compared with the product state when shikimate was used in soaking experiments.

Our goal was to use the substrate promiscuity of HCT to reduce lignin. In this attempt, we generated Arabidopsis lines that overproduce protocatechuate, a non-canonical acceptor and competitive inhibitor of HCT in vitro. The engineered plants accumulate approximatey 25-fold more protocatechuate than wild-type plants, and showed significant lignin reductions (31–37%) in biomass. Interestingly, transgenic lines expressing the *pobA* gene alone accumulated approximately 1.8-fold more protocatechuate than wild-type plants presumably from the conversion of the endogenous pool of *p*-hydroxybenzoate but showed no reduction of lignin content, suggesting that a threshold amount of protocatechuate is necessary to inhibit significantly HCT activity in vivo. Since lignin is reduced in the protocatechuate-overproducing plants, either the amount of *p*-coumaroyl protocatechuate produced by HCT is too low to sustain lignin biosynthesis, or *p*-coumaroyl protocatechuate is not metabolized further in the lignin biosynthetic pathway. In particular, it is not known whether C3′H can hydroxylate *p*-coumaroyl protocatechuate, and whether CSE would cleave the putative resulting *p*-caffeoyl protocatechuate. Neither *p*-coumaroyl

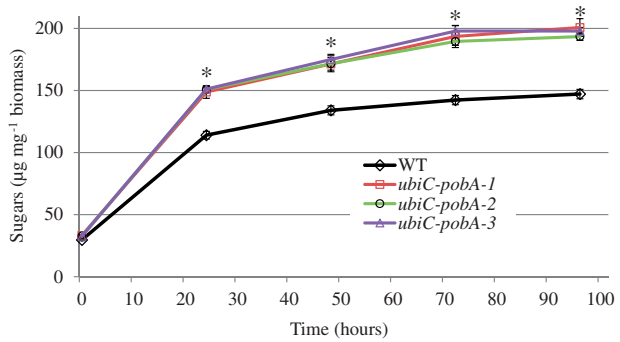


**Fig. 6** Saccharification of biomass from mature senesced stems of the wild type (WT) and *ubiC-pobA* transgenic lines. A 96 h time course of sugars released from pre-treated biomass digested with cellulase is shown. Values are means ± SE of six biological replicates ($n = 6$). Asterisks indicate significant differences from the WT using the unpaired Student's *t*-test ($P < 0.005$).

protocatechuate nor putative *p*-caffeoyl protocatechuate were detected in the metabolite extracts from *ubiC-pobA* transgenic plants, possibly because of their conjugation to other metabolites such as sugars, as was recently shown for other lignin oligomers (Dima et al. 2015).

Our dual transgene strategy consists of a two-step conversion of chorismate into protocatechuate. Steady-state levels of phenylalanine and salicylate, two metabolites derived from chorismate, are not significantly changed in the *ubiC*, *pobA* and *ubiC-pobA* transgenics compared with the wild type, suggesting that chorismate is not limiting in these lines, as previously hypothesized in the case of tobacco plants that express *ubiC* and show normal growth characteristics (Siebert et al. 1996, Viitanen et al. 2004). Therefore, the reduction of lignin observed only in the *ubiC-pobA* lines (and not in the *ubiC* single lines) is unlikely to be the consequence of phenylalanine depletion, although our data cannot rule out a possible slowing down of the metabolic flux. In addition, the height reduction observed in the *ubiC-pobA* lines at the mature stage is probably a consequence of lignin reduction rather than drastic changes in levels of salicylic acid, a metabolite whose overaccumulation in some transgenic plants often results in dwarf phenotypes (Rivas-San Vicente and Plasencia 2011).

In contrast to previous studies of plants in which HCT activity was down-regulated, the lignin composition of our transgenic lines does not show any enrichment in H units, possibly due to a lower degree of inhibition of activity and the consumption of *p*-coumaroyl-CoA by HCT for the formation of both *p*-coumaroyl protocatechuate and *p*-coumaroyl shikimate. Nevertheless, the increase of the S:G ratio in our transgenics, which results from the decrease of G units in favor of an increase in S units, is a lignin feature predicted by metabolic flux analysis in the case of HCT down-regulation, and was previously observed in plants affected in HCT activity (Chen and Dixon 2007, Ziebell et al. 2010, Vanholme et al, 2013b, Wang et al. 2014, Eudes et al. 2015). In addition, analysis of *HCT* transcript levels in the *ubiC-pobA* transgenic lines showed no major difference compared with the wild type (**Supplementary Fig. S10**), which is consistent with the hypothesis that protocatechuate affects the activity of HCT rather than its expression in the *ubiC-pobA* lines.

Engineering strategies for the overproduction of HCT non-canonical acceptors other than protocatechuate could be developed as alternative approaches to reduce lignin. For example, plant lines could be engineered to express anthranilate 3-hydroxylase, 2,3-dihydroxybenzoate synthase/dehydrogenase, salicylate 5-hydroxylases, 3-aminobenzoate synthase or 3-hydroxybenzoate synthase for the accumulation of 3-hydroxyanthranilate, 2,3-dihydroxybenzoate, 2,5-dihydroxybenzoate, 3-aminobenzoate or 3-hydroxybenzoate respectively, using the metabolites anthranilate, isochorismate, salicylate, 3-dehydroshikimate and chorismate as substrates (Gehring et al. 1997, Liu et al. 2010, Andexer et al. 2011, Hirayama et al. 2013, Zhang et al. 2013, Fang and Zhou 2014). It is interesting to note that very low amounts of 2,3- and 2,5-dihydroxybenzoates could be detected in our metabolite extracts from wild-type plants (~10 nmol $g^{-1}$ FW), whereas hydroxyanthranilates, 3-hydroxybenzoate and 3-aminobenzoate were below the detection limit, and, to our knowledge, have never been measured in plant extracts. With the exception of the occurrence of the phytoalexin *p*-coumaroyl 5-hydroxyanthranilate in oats (Collins 1989), *p*-coumaroyl conjugates of such phenolics have never been reported. Lastly, although catechol and hydroquinone are found in plants (Mageroy et al. 2012, Rychlińska and Nowak 2012), no corresponding *p*-coumaroyl esters have been described, maybe as a consequence of poor HCT activity towards these diphenols (**Supplementary Fig. S6**).

HCT seems to have appeared at the same time that plants began colonizing land. It is unclear why such promiscuity has been retained, and this question will require further study. However, a strategy of exploiting this substrate promiscuity of HCT offers a novel way to reduce lignin in plants. Because this enzymatic activity appears to be conserved among land plants, this strategy can be valuable to affect HCT activity in bioenergy crops for which no HCT gene has been cloned or for which multiple, functionally redundant copies are present. In this respect, particular attention should be paid to the spatio-temporal activity of the transgene promoters employed for the overproduction of HCT alternative substrates to limit possible growth defects associated with lignin reduction as observed in this study using Arabidopsis. Lastly, as we show here in the case of protocatechuate overproduction, such an approach has the potential to add value to plant biomass by increasing the amount of valuable metabolites utilized in the bio-based chemical industry (Linger et al. 2014).

## Materials and Methods

### Cloning of HCTs and activity assays using yeast

For the cloning of AtHCT and PpHCT1, total RNA (1 μg) from *A. thaliana* seedlings and total RNA (5 μg) from *P. patens* protonemal tissue were extracted using the Plant RNeasy extraction kit (Qiagen) and reverse-transcribed using the Transcriptor First Strand cDNA Synthesis Kit (Roche Applied Science). The cDNA preparations obtained were used to amplify AtHCT (GenBank accession No. NP_199704.1/At5g48930) and PpHCT1 (http://www.cosmoss.org, accession No. Pp3c2_29140V1.1; GenBank accession No. KU513965) using the oligonucleotides AtHCT-B1/AtHCT-B2 and PpHCT-B1/PpHCT-B2 (**Supplementary Table S6**), respectively, for cloning into the Gateway pDONR221 entry vector by BP recombination (Life Technologies). Gene sequences encoding for PtHCT6 (NCBI reference sequence XP_006368492.1), PvHCT2a (GenBank accession No. AGM90558.1), PrHCT (GenBank accession No. ABO52899.1) and SmHCT (NCBI reference sequence: XP_002991534.1), flanked with the *att*B1 (5′ end) and *att*B2 (3′ end) Gateway recombination sites, were synthesized for expression in yeast (GenScript) and cloned into the Gateway pDONR221 entry vector by BP recombination (Life Technologies). All six entry clones were LR recombined with the pDRf1-*4CL5*-GW vector (Eudes et al. 2011) to generate the constructs pDRf1-*4CL5-AtHCT*, pDRf1-*4CL5-PtHCT6*, pDRf1-*4CL5-PvHCT2a*, pDRf1-*4CL5-PrHCT*, pDRf1-*4CL5-SmHCT*, and pDRf1-*4CL5-PpHCT1*.

For HCT activity assays, the pDRf1-*4CL5-HCT* constructs and the control pDRf1-*4CL5* vector (Eudes et al. 2011) were transformed into the *Saccharomyces cerevisiae pad1* knockout (*MATa his3Δ1 leu2Δ0 met15Δ0 ura3Δ0 Δpad1*, ATCC 4005833) using the Frozen-EZ Yeast Transformation II Kit™ (Zymo Research Corporation) and selected on solid medium containing 1 × yeast nitrogen base (YNB) without amino acids (Difco 291940) supplemented with 3% glucose and 1 × dropout-uracil (CSM-ura; Sunrise Science Products). Overnight cultures from single colonies were grown in 2 × YNB

medium without amino acids (Difco) supplemented with 6% glucose and 2 × CSM-ura (Sunrise Science Products). Overnight cultures were used to inoculate 4 ml of fresh medium at an $OD_{600}$ = 0.15. Substrates were added to the medium 4 h later at a final concentration of 1 mM, and the cultures were grown for 24 h; *p*-coumarate was used as the donor, and the various acceptors tested (Sigma-Aldrich) are listed in **Supplementary Fig. S1**. For the detection of the *p*-coumaroyl conjugate products, an aliquot of the culture medium was collected, cleared by centrifugation (20,000 × *g* for 5 min at 4°C), mixed with an equal volume of 50% (v/v) methanol–water and filtered using Amicon Ultra centrifugal filters (3,000 Da MW cut-off regenerated cellulose membrane; EMD Millipore) prior to HPLC-electrospray ionization-time-of-flight MS (HPLC-ESI-TOF MS) analysis.

## Phylogenetic analysis

Multiple alignments on the full-length protein sequences were performed by ClustalW. A phylogenetic tree was generated with MEGA6 (Tamura et al. 2013) using the maximum likelihood method and default parameters.

## Heterologous expression, purification and activity of PvHCT2a

The pDONR221-PvHCT2a entry vector was LR recombined with the pDEST17 bacterial expression vector, which introduces an N-terminal 6 × His tag (Life Technologies). The construct was transferred into Rosetta 2 (DE3) chemically competent *E. coli* (EMD Milipore), according to the manufacturer's instructions. A single bacterial colony, grown on Luria–Bertani agar containing 100 μg $ml^{-1}$ carbenicillin and 30 μg $ml^{-1}$ chloramphenicol was used to inoculate a 5 ml liquid culture supplemented with the same antibiotic concentrations and grown overnight at 37°C. The overnight culture was used to inoculate a 0.5 liter Luria–Bertani culture at an $OD_{600}$ = 0.05 containing the same antibiotic concentrations and grown at 37 °C until it reached an $OD_{600}$ = 0.8–1.0. Expression was induced by the addition of 0.5 mM isopropyl-β-D-thiogalactopyranoside (IPTG), and the culture was transferred at 18 °C and grown for 24 h. The recombinant protein was affinity purified using a HIS-Select HF Nickel Affinity Gel (Sigma-Aldrich) according to the manufacturer's instructions and buffer-exchanged with 40 mM Tris buffer pH 7.5 using Amicon Ultra centrifugal filters (30,000 Da MW cut-off regenerated cellulose membrane; EMD Millipore). Purity and integrity were verified by SDS–PAGE, and the recombinant protein was stored at −20 °C in 40 mM Tris buffer pH 7.5, containing 10% (v/v) glycerol.

In vitro transferase assays were performed at 30 °C for 15 min in 40 μl reactions containing 50 mM Tris buffer pH 7.5, 1 mM dithiothreitol (DTT), 400 μM *p*-coumaroyl-CoA (MicroCombiChem e.K.), 120 ng of recombinant PvHCT2a protein and 1 mM of various acyl acceptors. Similar conditions were used to obtain substrate saturation curves except that the incubation time was reduced to 2 min and the concentration of the acyl acceptors varied from 0 to 6.4 or 12.8 mM. For the competitive inhibition experiment, assays were performed at 30 °C for 15 min in 40 μl reactions containing 50 mM Tris buffer pH 7.5, 400 μM *p*-coumaroyl-CoA, 400 μM shikimate and 120 ng of recombinant PvHCT2a protein without (control) or with 0.4–1.6 mM of various acyl acceptors. All reactions were terminated by adding 40 μl of 50% (v/v) cold methanol–water and kept at −20 °C until HPLC-ESI-TOF MS analysis.

For structural study, a PvHCT2a sequence was synthesized for expression in *E. coli* (GenScript), amplified using the oligonucleotides PvHCT2a-infus-fw/PvHCT2a-infus-rv (**Supplementary Table S6**) and cloned into a *Bam*HI/*Nde*I-digested pSKB3 vector using the In-Fusion HD cloning kit (Clontech). The construct was transferred into BL21 (DE3) chemically competent *E. coli* (EMD Milipore), according to the manufacturer's instructions. A single bacterial colony, grown on Luria–Bertani agar containing 50 μg $ml^{-1}$ kanamycin was used to inoculate a 50 ml liquid culture supplemented with the same antibiotic concentrations and grown overnight at 37 °C. The overnight culture was used to inoculate a 3 liter Luria–Bertani culture containing the same antibiotic concentration and grown at 37 °C until it reached an $OD_{600}$ = 0.8. Expression was induced by the addition of 0.5 mM IPTG, and the culture was transferred at 18 °C and grown for 24 h. Cell paste was lysed in 50 mM Tris–HCl pH 8.0, 300 mM NaCl and 30 mM imidazole, and loaded onto a 5 ml Histrap column on an AKTA FPLC. The column was washed to baseline prior to elution with a gradient of 0–100% buffer 50 mM Tris–HCl pH 8.0, 300 mM NaCl and 500 mM imidazole in 20 column volumes. The cleanest elution fractions were pooled and dialyzed back into the lysis buffer with the addition of TEV protease to remove the 6His-tag. The cleaved material was applied again through a 5 ml Histrap column on the AKTA FPLC to separate the cleaved PvHCT2a from other components. The purified PvHCT2a was then dialyzed into 50 mM Tris–HCl pH 8.0 and 20 mM NaCl prior to concentration for crystallographic studies.

## Crystallization of PvHCT2a in complex with ligands

The final concentration of PvHCT2a used for crystallization trials was 12 mg $ml^{-1}$. The PvHCT2a apoenzyme sample was screened using the sparse matrix method (Jancarik and Kim 1991) with a Phoenix Robot (Art Robbins Instruments) and the following crystallization screens: Crystal Screen, SaltRx, PEG/Ion, Index and PEGRx (Hampton Research) and Berkeley Screen [Lawrence Berkeley National Laboratory (LBNL)]. Crystals of PvHCT2a apoenzyme were found in 0.2 M lithium sulfate, 0.1 M Tris–HCl pH 8.5 and 25% (w/v) polyethylene glycol 3,350. Crystals of PvHCT2a in complex with *p*-coumaroyl-CoA–shikimate and *p*-coumaroyl-CoA–protocatechuate were obtain by soaking PvHCT2a apoenzyme crystals using 5 mM *p*-coumaroyl-CoA and 5 mM shikimate or protocatechuate solutions for 3 h. Crystals of PvHCT2a apoenzyme were obtained after 1 d by the sitting-drop vapor diffusion method, with the drops consisting of a mixture of 0.5 μl of protein solution and 0.5 μl of reservoir solution.

## X-ray data collection and structure determination

The crystals of PvHCT2a–*p*-coumaroyl-CoA–shikimate and PvHCT2a–*p*-coumaroyl-CoA–protocatechuate were placed in a reservoir solution containing 20% (v/v) glycerol, then flash-frozen in liquid nitrogen. The X-ray data sets for PvHCT2a–*p*-coumaroyl-CoA–shikimate and PvHCT2a–*p*-coumaroyl-CoA–protocatechuate were collected at the Berkeley Center for Structural Biology beamlines 8.2.1 and 8.2.2 of the Advanced Light Source at LBNL. The diffraction data were recorded using an ADSC-Q315r detector. The data sets were processed using the program HKL-2000 (Otwinowski and Minor 1997).

The PvHCT2a–*p*-coumaroyl-CoA–shikimate structure was determined by the molecular-replacement method with the program PHASER (McCoy et al. 2007) using the SbHCT structure (PDB ID 4KE4) (Walker et al. 2013) as a search model. The PvHCT2a–*p*-coumaroyl–CoA-shikimate structure was used as a search model to solve the PvHCT2a–*p*-coumaroyl–CoA-protocatechuate structure. Structure refinement was performed using the phenix.refine program (Afonine et al. 2012). Manual rebuilding using COOT (Emsley and Cowtan 2004) and the addition of water molecules allowed construction of the final model. Five percent of the data were randomly selected for cross-validation. The final model of PvHCT2a–*p*-coumaroyl-CoA–shikimate and PvHCT2a–*p*-coumaroyl-CoA–protocatechuate have *R* and $R_{free}$ factors of 15.9%/18.6% and 17.9%/20.5%, respectively. Root-mean-square deviation differences from ideal geometry for bond lengths, angles and dihedrals were calculated with Phenix (Adams et al. 2010). The overall stereochemical quality of the final models was assessed using the program MolProbity (Davis et al. 2007).

## Plant material and growth conditions

Seeds of wild-type and transgenic *A. thaliana* (ecotype Columbia, Col-0) lines were germinated directly on soil. Growing conditions were 150 μmol $m^{-2}$ $s^{-1}$, 22 °C, 60% humidity and 14 h of light per day. Selection of $T_2$ transgenic plants and identification of homozygous lines, for which the $T_3$ progeny were not segregating on antibiotic, was made on Murashige and Skoog vitamin medium (PhytoTechnology Laboratories), supplemented with 1% sucrose, 0.8% agar and 50 μg $ml^{-1}$ kanamycin.

## HCT activity assays in Arabidopsis

Total proteins were extracted from Arabidopsis stems as previously described (Vanholme et al. 2013b). Briefly, stems of 5-week-old wild-type plants were frozen in liquid nitrogen and ground into a fine powder. Total proteins from approximately 500 mg of stem powder were extracted at 4 °C with 1 ml of extraction buffer consisting of 20 mM Tris–HCl pH 7.5 containing 10 mM DTT, 15% glycerol, 1% insoluble polyvinylpolypyrrolidone (PVPP) and 1 × protease inhibitor cocktail (Roche). Total proteins were quantified using the Bradford method (Bradford

1976). HCT activity assays were performed at 30 °C for 30 min in 40 µl reactions containing 50 mM Tris–HCl pH 7.5, 400 µM *p*-coumaroyl-CoA, 400 µM shikimate and 12 µg of total proteins without (control) or with 400 µM of various acyl acceptors. All reactions were terminated by adding 40 µl of 50% (v/v) cold methanol–water and kept at −20 °C until HPLC-ESI-TOF MS analysis.

## Construction of binary vectors

Generation of the pTKan-*pCesa4*::GWR1R2 destination vector was previously described (Eudes et al. 2012). To generate the pTKan-*pCesa4*::*schl-ubiC* construct, a gene sequence encoding ubiC from *E. coli* (GenBank accession No. CAA47181.1) containing the encoding sequence of a plastid targeting signal (SCHL; Lebrun et al. 1992) and flanked with the Gateway *att*B1 (5′ end) and *att*B4 (3′ end) recombination sites was synthesized for expression in Arabidopsis (**Supplementary Data** S1) (GenScript). The sequence was amplified by PCR to replace the Gateway *att*B4 (3′ end) by the *att*B2 recombination site and cloned into the Gateway pDONR221-P1P2 entry vector by BP recombination (Life Technologies). A sequence-verified entry clone was LR recombined with the pTKan-*pCesa4*::GWR1R2 vector to generate the pTKan-*pCesa4*::*schl-ubiC* construct.

Generation of the pTKan-*pC4H*::*schl*-GWR3R2 destination vector was previously described (Eudes et al. 2015). To generate the pTKan-*pC4H*::*schl-pobA* construct, a gene sequence encoding pobA from *P. aeruginosa* (GenBank accession No. AAG03636.1) flanked with the Gateway *att*B3 (5′ end) and *att*B2 (3′ end) recombination sites was synthesized for expression in Arabidopsis (**Supplementary Data S1**) (GenScript) and cloned into the Gateway pDONR221-P3P2 entry vector by BP recombination (Life Technologies). An entry clone was LR recombined with the pTKan-*pC4H*::*schl*-GWR3R2 vector to generate the pTKan-*pC4H*::*schl-pobA* construct.

A multisite LR recombination (Life Technologies) using the pDONR221-P1-*schl*::*ubiC*-P4, pDONR221-L4R-*tg7-pC4H*::*schl*-L3R (Eudes et al. 2015) and pDONR221-P3-*pobA*-P2 entry vectors and the pTKan-*pCesa4*::GWR1R2 destination vector was performed to generate the pTKan-*pCesa4*::*schl-ubiC-pC4H*::*schl-pobA* construct.

All constructs were introduced into wild-type (Col-0) Arabidopsis plants via *Agrobacterium*-mediated transformation (Bechtold and Pelletier 1998).

## RNA extraction and RT–PCR

Total RNA (1 µg) were extracted from stems of 5-week-old wild-type and $T_3$ homozygous transgenic lines using the Plant RNeasy extraction kit (Qiagen) and reverse-transcribed using the Transcriptor First Strand cDNA Synthesis Kit (Roche Applied Science). The cDNA preparations obtained were quality-controlled using *tub8*-specific oligonucleotides, and the *pobA*, *ubiC* and *AtHCT* transcripts were detected using specific oligonucleotides listed in **Supplementary Table S6**. For the PCR, OneTaq (New England Biolabs) was used according to the manufacturer's instructions, with 1 min of elongation time and 60 °C for the annealing temperature. Thirty (for *pobA* and *ubiC* expression) or 25 (for *AtHCT* expression) PCR cycles were used to amplify the DNA fragments.

## Plant metabolite extraction

Arabidopsis stems of 6-week-old wild-type and $T_3$ homozygous transgenic lines were collected in liquid nitrogen and stored at −80 °C until further utilization. Prior to metabolite extraction, collected stems were pulverized in liquid nitrogen. For extraction of methanol-soluble metabolites, 200–300 mg of frozen stem powder was mixed with 1 ml of 80% (v/v) methanol–water and shaken at 1,400 r.p.m. for 15 min at 70 °C. The mixture was cleared by centrifugation for 5 min at 20,000 × *g*. This step was repeated four times. Extracts were pooled and cleared once more by centrifugation (5 min, 20,000 × *g*), mixed with 2 ml of analytical grade water and filtered using Amicon Ultra centrifugal filters (10,000 Da MW cut-off regenerated cellulose membrane; EMD Millipore). Phenylalanine was quantified in the filtered extracts using HPLC-ESI-TOF MS analysis. For measurement of 4-hydroxybenzoate, protocatechuate and salicylic acid, an aliquot of the filtered extracts was dried under vacuum, resuspended with 1 N HCl and incubated at 95 °C for 3 h. The mixture was subjected to three ethyl acetate partitioning steps. Ethyl acetate fractions were pooled, dried in vacuo and resuspended in 50% (v/v) methanol–water prior to HPLC-ESI-TOF MS analysis.

## Metabolite analyses

Metabolites were analyzed using HPLC-ESI-TOF MS as previously described (Eudes et al. 2013, Eudes et al. 2015). Protocatechuate, 4-hydroxybenzoate, phenylalanine, and salicylic acid were quantified via 10-point calibration curves of authentic standard compounds for which the $R^2$ coefficients were ≥ 0.99. For the identification of the *p*-coumaroyl conjugates, the measured masses agreed with the expected theoretical masses within < 5 p.p.m. mass error.

## Lignin content and composition

The biomass from senesced mature stems of wild-type plants and $T_3$ homozygous transgenic lines was used to determine lignin content and composition. Soluble extracts from stem biomass samples were extracted sequentially by sonication (20 min) with 80% ethanol (three times), acetone (once), chloroform–methanol (1 : 1, v/v, once) and acetone (once). The standard NREL biomass protocol was used to measure the lignin content (Sluiter et al. 2008). The chemical composition of lignin was analyzed by pyrolysis–GC/MS as previously described (Del Rio et al. 2012, Eudes et al. 2015).

## Cell wall pretreatments and saccharification

Ball-milled senesced mature stems (10 mg) were mixed with 340 µl of NaOH (0.25%, w/v), shaken at 1,400 r.p.m. (30 °C, 30 min) and autoclaved at 120 °C for 1 h for dilute alkali pre-treatment. Saccharification was initiated by adding 650 µl of 100 mM sodium citrate buffer pH 5.0 containing 80 µg ml$^{-1}$ tetracycline and 1% (w/w) Cellic CTec2 cellulase (Novozymes). At $t = 0$ and after 24, 48, 72 and 96 h of incubation at 50 °C with shaking (800 r.p.m.), samples were centrifuged (20,000 × *g*, 2 min) and 10 µl of the supernatant was collected for measurement of reducing sugars using the 3,5-dinitrosalicylic acid assay and glucose solutions as standards (Miller 1959).

## Data deposition

The atomic co-ordinates and structure factors of PvHCT2a–*p*-coumaryl-CoA–shikimate and PvHCT2a–*p*-coumaryl-CoA–protocatechuate complexes have been deposited in the Protein Data Bank, with PDB ID codes 5FAL and 5FAN, respectively.

## Supplementary data

**Supplementary data** are available at PCP online.

## Funding

This work was part of the DOE Joint BioEnergy Institute (http://www.jbei.org) supported by the U. S. Department of Energy, Office of Science, Office of Biological and Environmental Research, through contract DE-AC02-05CH11231 between Lawrence Berkeley National Laboratory and the U.S. Department of Energy. The Berkeley Center for Structural Biology is supported in part by the National Institutes of Health, National Institute of General Medical Sciences. The Advanced Light Source is supported by the Director, Office of Science, Office of Basic Energy Sciences, of the U.S. Department of Energy under Contract No. DE-AC02-05CH11231. The United States Government retains and the publisher, by accepting the article for publication, acknowledges that the United States Government retains a non-exclusive, paid-up, irrevocable, world-wide license to publish or reproduce the published form of this manuscript, or allow others to do so, for United States Government purposes.

## Acknowledgements

The authors thank Noppadon Sathitsuksanoh for assistance with the pyrolysis–GC/MS, Tess Scavuzzo-Duggan for providing *P. patens* protonemal tissue, Dr. Nigel W. Moriarty for helpful analysis of the ligand geometry and restraints, Novozymes for providing Cellic CTec2, and Sabin Russell for editing this manuscript. We are also grateful to the staff of the Berkeley Center for Structural Biology at the Advanced Light Source of Lawrence Berkeley National Laboratory.

## Disclosures

J.D.K. has financial conflicts of interest in Amyris, LS9, and Lygos. D.L. has financial conflicts of interest in Afingen. All other authors have no conflicts of interest to declare.

## References

Andexer, J.N., Kendrew, S.G., Nur-e-Alam, M., Lazos, O., Foster, T.A., Zimmermann, A.S., et al. (2011) Biosynthesis of the immunosuppressants FK506, FK520, and rapamycin involves a previously undescribed family of enzymes acting on chorismate. *Proc. Natl. Acad. Sci. USA* 108: 4776–4781.

Adams, P.D., Afonine, P.V., Bunkoczi, G., Chen, V.B., Davis, I.W., Echols, N., et al. (2010) PHENIX: a comprehensive Python-based system for macromolecular structure solution. *Acta Crystallogr. D Biol. Crystallogr.* 66: 213–221.

Afonine, P.V., Grosse-Kunstleve, R.W., Echols, N., Headd, J.J., Moriarty, N.W., Mustyakimov, M., et al. (2012) Towards automated crystallographic structure refinement with phenix.refine. *Acta Crystallogr. D Biol. Crystallogr.* 68: 352–367.

Bechtold, N. and Pelletier, G. (1998) In planta *Agrobacterium*-mediated transformation of adult Arabidopsis thaliana plants by vacuum infiltration. *Methods Mol. Biol.* 82: 259–266.

Boerjan, W., Ralph, J. and Baucher, M. (2003) Lignin biosynthesis. *Annu. Rev. Plant Biol.* 54: 519–546.

Bradford, M.M. (1976) A rapid and sensitive method for the quantitation of microgram quantities of protein utilizing the principle of protein–dye binding. *Anal. Biochem.* 72: 248–254.

Chen, F. and Dixon, R.A. (2007) Lignin modification improves fermentable sugar yields for biofuel production. *Nat. Biotechnol.* 25: 759–761.

Collins, F.W. (1989) Oat phenolics: avenanthramides, novel substituted N-cinnamoylanthranilate alkaloids from oat groats and hulls. *J. Agric. Food Chem.* 37: 60–66.

D'Auria, J.C. (2006) Acyltransferases in plants: a good time to be BAHD. *Curr. Opin. Plant Biol.* 9: 331–340.

Davis, I.W., Leaver-Fay, A., Chen, V.B., Block, J.N., Kapral, G.J., Wang, X., et al. (2007) MolProbity: all-atom contacts and structure validation for proteins and nucleic acids. *Nucleic Acids Res.* 35: W375–W383.

Del Río, J.C., Rencoret, J., Prinsen, P., Martínez, A.T., Ralph, J. and Gutiérrez, A. (2012) Structural characterization of wheat straw lignin as revealed by analytical pyrolysis, 2D-NMR, and reductive cleavage methods. *J. Agric. Food Chem.* 60: 5922–5935.

Dima, O., Morreel, K., Vanholme, B., Kim, H., Ralph, J. and Boerjan, W. (2015) Small glycosylated lignin oligomers are stored in Arabidopsis leaf vacuoles. *Plant Cell* 27: 695–710.

Emsley, P. and Cowtan, K. (2004) Coot: model-building tools for molecular graphics. *Acta Crystallogr. D Biol. Crystallogr.* 60: 2126–2132.

Escamilla-Treviño, L.L., Shen, H., Hernandez, T., Yin, Y., Xu, Y. and Dixon R.A. (2014) Early lignin pathway enzymes and routes to chlorogenic acid in switchgrass (Panicum virgatum L.). *Plant Mol. Biol.* 84: 565–756.

Eudes, A., Baidoo, E.E., Yang, F., Burd, H., Hadi, M.Z., Collins, F.W., et al. (2011) Production of tranilast [N-(3′,4′-dimethoxycinnamoyl)-anthranilic acid] and its analogs in yeast *Saccharomyces cerevisiae*. *Appl. Microbiol. Biotechnol.* 89: 989–1000.

Eudes, A., George, A., Mukerjee, P., Kim, J.S., Pollet, B., Benke, P.I., et al. (2012) Biosynthesis and incorporation of side-chain-truncated lignin monomers to reduce lignin polymerization and enhance saccharification. *Plant Biotechnol. J.* 10: 609–620.

Eudes, A., Juminaga, D., Baidoo, E.E., Collins, F.W., Keasling, J.D. and Loqué, D. (2013) Production of hydroxycinnamoyl anthranilates from glucose in *Escherichia coli*. *Microb. Cell Fact.* 12: 62.

Eudes, A., Sathitsuksanoh, N., Baidoo, E.E., George, A., Liang, Y., Yang, F., et al. (2015) Expression of a bacterial 3-dehydroshikimate dehydratase reduces lignin content and improves biomass saccharification efficiency. *Plant Biotechnol. J.* 13: 1241–1250.

Erxleben, A., Gessler, A., Vervliet-Scheebaum, M. and Reski, R. (2012) Metabolite profiling of the moss *Physcomitrella patens* reveals evolutionary conservation of osmoprotective substances. *Plant Cell Rep.* 31: 427–436.

Fang, T. and Zhou, N.Y. (2014) Purification and characterization of salicylate 5-hydroxylase, a three-component monooxygenase from *Ralstonia sp.* strain U2. *Appl. Microbiol. Biotechnol.* 98: 671–679.

Franke, R., Hemm, M.R., Denault, J.W., Ruegger, M.O., Humphreys, J.M. and Chapple C. (2002) Changes in secondary metabolism and deposition of an unusual lignin in the ref8 mutant of Arabidopsis. *Plant J.* 30: 47–59.

George, K.W., Alonso-Gutierrez, J., Keasling, J.D. and Lee, T.S. (2015) Isoprenoid drugs, biofuels, and chemicals—artemisinin, farnesene, and beyond. *Adv. Biochem. Eng. Biotechnol.* 148: 355–389.

Gehring, A.M., Bradley, K.A. and Walsh, C.T. (1997) Enterobactin biosynthesis in *Escherichia coli*: isochorismate lyase (EntB) is a bifunctional enzyme that is phosphopantetheinylated by EntD and then acylated by EntE using ATP and 2,3-dihydroxybenzoate. *Biochemistry* 36: 8495–8503.

Hirayama, A., Eguchi, T. and Kudo, F. (2013) A single PLP-dependent enzyme PctV catalyzes the transformation of 3-dehydroshikimate into 3-aminobenzoate in the biosynthesis of pactamycin. *Chembiochem* 14: 1198–203.

Hoffmann, L., Besseau, S., Geoffroy, P., Ritzenthaler, C., Meyer, D., Lapierre, C., et al. (2004) Silencing of hydroxycinnamoyl-coenzyme A shikimate/quinate hydroxycinnamoyltransferase affects phenylpropanoid biosynthesis. *Plant Cell* 16: 1446–1465.

Hoffmann, L., Maury, S., Martz, F., Geoffroy, P. and Legrand, M. (2003) Purification, cloning, and properties of an acyltransferase controlling shikimate and quinate ester intermediates in phenylpropanoid metabolism. *J. Biol. Chem.* 278: 95–103.

Jancarik, J. and Kim, S.-H. (1991) Sparse matrix sampling: a screening method for crystallization of proteins. *J. Appl. Crystallogr.* 24: 409–411.

Kim, B.G., Kim, I.A. and Ahn, J.H. (2011) Characterization of hydroxycinnamoyl-coenzyme A shikimate hydroxycinnamoyltransferase from Populus euramericana. *J. Korean Soc. Appl. Biol. Chem.* 54: 817–821.

Lallemand, L.A., Zubieta, C., Lee, S.G., Wang, Y., Acajjaoui, S., Timmins, J., et al. (2012) A structural basis for the biosynthesis of the major chlorogenic acids found in coffee. *Plant Physiol.* 160: 249–260.

Landmann, C., Hücherig, S., Fink, B., Hoffmann, T., Dittlein, D., Coiner, H.A., et al. (2011) Substrate promiscuity of a rosmarinic acid synthase from lavender (*Lavandula angustifolia* L.). *Planta* 234: 305–320.

Lebrun, M., Leroux, B. and Sailland, A. (1992) Gène chimère pour la transformation des plantes. European patent application. Patent Application No. EP 508909A1.

Linger, J.G., Vardon, D.R., Guarnieri, M.T., Karp, E.M., Hunsinger, G.B., Franden, M.A., et al. (2014) Lignin valorization through integrated

biological funneling and chemical catalysis. *Proc. Natl. Acad. Sci. USA* 111: 12013–12018.

Liu, X., Dong, Y., Li, X., Ren, Y., Li, Y., Wang, W., et al. (2010) Characterization of the anthranilate degradation pathway in *Geobacillus thermodenitrificans* NG80-2. *Microbiology* 156: 589–595.

McCoy, A.J., Grosse-Kunstleve, R.W., Adams, P.D., Winn, M.D., Storoni, L.C. and Read, R.J. (2007) Phaser crystallographic software. *J. Appl. Crystallogr.* 40: 658–674.

Mageroy, M.H., Tieman, D.M., Floystad, A., Taylor, M.G. and Klee, H.J. (2012) A *Solanum lycopersicum* catechol-O-methyltransferase involved in synthesis of the flavor molecule guaiacol. *Plant J.* 69: 1043–1051.

Miller, G. (1959) Use of dinitrosalicylic acid reagent for determination of reducing sugar. *Anal. Chem.* 31: 426–428.

Moglia, A., Comino, C., Lanteri, S., de Vos, R., de Waard, P., van Beek, T.A., et al. (2010) Production of novel antioxidative phenolic amides through heterologous expression of the plant's chlorogenic acid biosynthesis genes in yeast. *Metab. Eng.* 12: 223–232.

Molina, I. and Kosma, D. (2014) Role of HXXXD-motif/BAHD acyltransferases in the biosynthesis of extracellular lipids. *Plant Cell Rep.* 34: 587–601.

Otwinowski, Z. and Minor, W. (1997) Processing of X-ray diffraction data collected in oscillation mode. *Methods Enzymol.* 276: 307–326.

Rivas-San Vicente, M. and Plasencia, J. (2011) Salicylic acid beyond defence: its role in plant growth and development. *J. Exp. Bot.* 62: 3321–3338.

Rychlińska, I. and Nowak, S. (2012) Quantitative determination of arbutin and hydroquinone in different plant materials by HPLC. *Not. Bot. Horti Agrobot.* 40: 109–113.

Sander, M. and Petersen, M. (2011) Distinct substrate specificities and unusual substrate flexibilities of two hydroxycinnamoyltransferases, rosmarinic acid synthase and hydroxycinnamoyl-CoA:shikimate hydroxycinnamoyl-transferase, from Coleus blumei Benth. *Planta* 233: 1157–1171.

Shadle, G., Chen, F., Srinivasa Reddy, M.S., Jackson, L., Nakashima, J. and Dixon, R.A. (2007) Down-regulation of hydroxycinnamoyl CoA:shikimate hydroxycinnamoyl transferase in transgenic alfalfa affects lignification, development and forage quality. *Phytochemistry* 68: 1521–1529.

Shen, H., Mazarei, M., Hisano, H., Escamilla-Trevino, L., Fu, C., Pu, Y., et al. (2013) A genomics approach to deciphering lignin biosynthesis in switchgrass. *Plant Cell* 25: 4342–4361.

Shi, R., Sun, Y.H., Li, Q., Heber, S., Sederoff, R. and Chiang, V.L. (2010) Towards a systems approach for lignin biosynthesis in *Populus trichocarpa*: transcript abundance and specificity of the monolignol biosynthetic genes. *Plant Cell Physiol.* 51: 144–146.

Siebert, M., Sommer, S., Li, S.M., Wang, Z.X., Severin, K. and Heide, L. (1996) Genetic engineering of plant secondary metabolism. Accumulation of 4-hydroxybenzoate glucosides as a result of the expression of the bacterial *ubiC* gene in tobacco. *Plant Physiol.* 112: 811–819.

Sluiter, A., Hames, B., Ruiz, R., Scarlata, C. and Sluiter, J. (2008) Determination of structural carbohydrates and lignin in biomass. *In* Laboratory Analytical Procedure (Technical Report, NREL/TP-510-42618), National Renewable Energy Laboratory, Golden, CO.

Tamura, K., Stecher, G., Peterson, D., Filipski, A. and Kumar S (2013) MEGA6: molecular evolutionary genetics analysis version 6.0. *Mol. Biol. Evol.* 30: 2725–2729.

Tohge, T., Watanabe, M., Hoefgen, R. and Fernie, A.R. (2013) The evolution of phenylpropanoid metabolism in the green lineage. *Crit. Rev. Biochem. Mol. Biol.* 48: 123–152.

Vanholme, B., Cesarino, I., Goeminne, G., Kim, H., Marroni, F., Van Acker, R., et al. (2013b) Breeding with rare defective alleles (BRDA): a natural *Populus nigra* HCT mutant with modified lignin as a case study. *New Phytol.* 198: 765–76.

Vanholme, R., Cesarino, I., Rataj, K., Xiao, Y., Sundin, L., Goeminne, G., et al. (2013a) Caffeoyl shikimate esterase (CSE) is an enzyme in the lignin biosynthetic pathway in Arabidopsis. *Science* 341: 1103–1106.

Vickers, C.E., Klein-Marcuschamer, D. and Krömer, J.O. (2012) Examining the feasibility of bulk commodity production in *Escherichia coli*. *Biotechnol. Lett.* 34: 585–595.

Viitanen, P.V., Devine, A.L., Khan, M.S., Deuel, D.L., Van Dyk, D.E. and Daniell, H. (2004) Metabolic engineering of the chloroplast genome using the *Echerichia coli ubiC* gene reveals that chorismate is a readily abundant plant precursor for p-hydroxybenzoic acid biosynthesis. *Plant Physiol.* 136: 4048–4060.

Wagner, A., Ralph, J., Akiyama, T., Flint, H., Phillips, L., Torr, K., et al. (2007) Exploring lignification in conifers by silencing hydroxycinnamoyl-CoA:shikimate hydroxycinnamoyltransferase in *Pinus radiata*. *Proc. Natl. Acad. Sci. USA* 104: 11856–11861.

Walker, A.M., Hayes, R.P., Youn, B., Vermerris, W., Sattler, S.E. and Kang, C. (2013) Elucidation of the structure and reaction mechanism of sorghum hydroxycinnamoyltransferase and its structural relationship to other coenzyme a-dependent transferases and synthases. *Plant Physiol.* 162: 640–651.

Wang, J.P., Naik, P.P., Chen, H.C., Shi, R., Lin, C.Y., Liu, J., et al. (2014) Complete proteomic-based enzyme reaction and inhibition kinetics reveal how monolignol biosynthetic enzyme families affect metabolic flux and lignin in *Populus trichocarpa*. *Plant Cell* 26: 894–914.

Weng, J.K., Akiyama, T., Bonawitz, N.D., Li, X., Ralph, J. and Chapple, C. (2010) Convergent evolution of syringyl lignin biosynthesis via distinct pathways in the lycophyte Selaginella and flowering plants. *Plant Cell* 22: 1033–1045.

Weng, J.K. and Noel, J.P. (2013) Chemodiversity in *Selaginella*: a reference system for parallel and convergent metabolic evolution in terrestrial plants. *Front. Plant Sci.* 4: 119.

Xu, Z., Zhang, D., Hu, J., Zhou, X., Ye, X., Reichel, K.L., et al. (2009) Comparative genome analysis of lignin biosynthesis gene families across the plant kingdom. *BMC Bioinformatics* 10 (Suppl. 11): S3.

Zeng, Y., Zhao, S., Yang, S. and Ding, S.Y. (2014) Lignin plays a negative role in the biochemical process for producing lignocellulosic biofuels. *Curr. Opin. Biotechnol.* 27: 38–45.

Zhang, K., Halitschke, R., Yin, C., Liu, C.J. and Gan, S.S. (2013) Salicylic acid 3-hydroxylase regulates *Arabidopsis* leaf longevity by mediating salicylic acid catabolism. *Proc. Natl. Acad. Sci. USA* 110: 14807–14812.

Ziebell, A., Gracom, K., Katahira, R., Chen, F., Pu, Y., Ragauskas, A., et al. (2010) Increase in 4-coumaryl alcohol units during lignification in alfalfa (*Medicago sativa*) alters the extractability and molecular weight of lignin. *J. Biol. Chem.* 285: 38961–38968.